Engineering Science and Military Technologies
Volume (8) - Issue (1) - Mar 2024
ISSN: 2357- 0954
DOI:10.21608/EJMTC.2023.168437.1236

Experimental investigation and performance enhancement of swing check valves

Original Article

Ibrahim Ali Ismail[1], Mohamed Yehia Zakaria[2], El-Sayed El-Agouz[1]

[1]Department of Mechanical Power Engineering, Tanta University, Tanta, [2]Department of Aircraft Mechanics, Military Technical College, Cairo, Egypt

Keywords:
Check valve, non-return, reversed flow, swing, slam.

Corresponding Author:
Zakaria, Mohamed Yehia, Department of Aircraft Mechanics, Military Technical College, **Tel.:** +201033442200, **Email:** zakaria@mtc.edu.eg

Abstract
The swing check valve (SCV) is a type of check valves or non-return valves that allows the fluid to flow in one direction only. The main goal of this research is devoted to enhance the SCV performance by accelerating the SCV closure, thus reducing the amount of reversed flow through the valve before it is fully closed. This will be carried out only by modifying the design of the SCV itself and without using any external devices like springs or external attached masses. A wafer type SCV is used as a case study to investigate its transient closing characteristics; flapper's angle, reversed flow through the SCV and pressure rise due to the valve closure. With the aid of numerical simulation, five of ten suggested modifications are chosen and 3D printed to be tested experimentally versus the original/reference design. The experimental investigation shows that two of the five designs close faster with less reversed flow than the original/basic design.

1. INTRODUCTION

Check valves are widely used in nuclear plants for many purposes[1]. The swing check valve (SCV) is one of the most used types of check valves in nuclear plants[2]. The major advantages of the SCV are its low pressure drop, availability in wide range of sizes, simple design and ease of maintenance.On the other hand, its major disadvantage is the slow closure that allows a considerable amount of reversed flow to pass through the SCV before it is fully closed. Failure of the SCV may cause catastrophic maintenance problems such as water hammering, damaging flow system components[1] and fluid leakage. Therefore, many studies are concerned of the problems associated with SCV operation[3] and different condition-monitoring techniques[4] that warn the operator before the SCV failure. Another sort of studies is concerned with the dynamic performance of the SCV either experimentally[5], mathematically[6] and recently using computational fluid dynamics (CFD)[7].

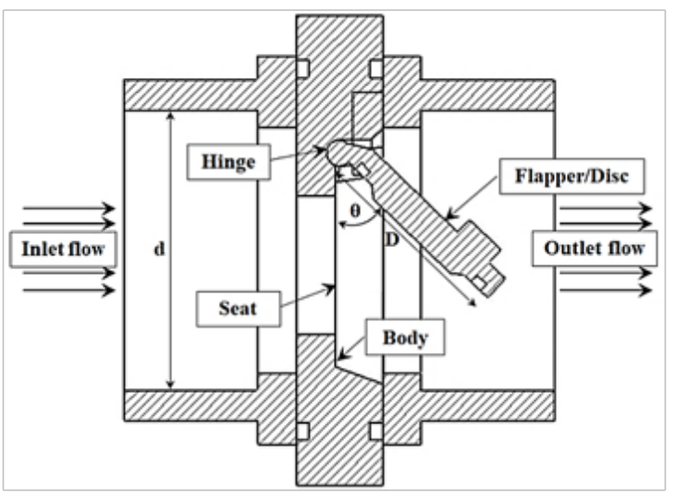

Fig. 1: Basic construction of a wafer type SCV.

The simple design of the SCV that is shown in Figure 1 encouraged other researchers to develop extensions of this basic design to achieve a better performance. Knoedler[8] investigated a classical SCV used in low pressure coolant injection systems. The interface between the flapper and its seat was repeatedly damaged. He found that the disk did not always completely cover the seat area. Therefore, he modified the interface between the seat and the body into a rugged flange body design. Mochizuki[9] introduced four SCV modifications to improve closure characteristics. He added an orifice upstream of the valve, welded a weight on the valve disc and a paddle on the disc shaft to confine water and provide a damping action.

Li *et al.*[7] have enlarged the bottom of a SCV body; this modification resulted in reducing swirl vortices, flow separation, negative pressure zones as well as energy losses. Shin *et al.*[10] found that in the optimized power reactor (OPR), the SCV failure contributes to the failure of the auxiliary feed water system (AFWS) by about 74.3% in some accidents scenarios. Therefore, they modified the design of the SCV from a passive operated (naturally driven by the flow) to be an active element (driven by an externally powered mechanism). Their analysis showed that the AFWS unreliability due to the failure of the SCV is reduced by two to four orders of magnitude. With this design modification, the contribution of the failure of the SCV to AFWS unreliability became less than 0.5%.

1.1. Objective

In the present work, a case study is suggested by using a commercial on shelf SCV. This SCV is investigated analytically[11] and experimentally. Then, the basic parameters such as (flow velocity and pressure) are taken as input parameters for the steady-state numerical simulation. Consequently, the original SCV is simulated versus ten proposed extensions to reduce the SCV closing time and the reversed flow through the SCV. Eventually, five designs are selected for manufacturing with 3D printing technology and experimental investigation. Figure 2 summarizes the flow of the current work.

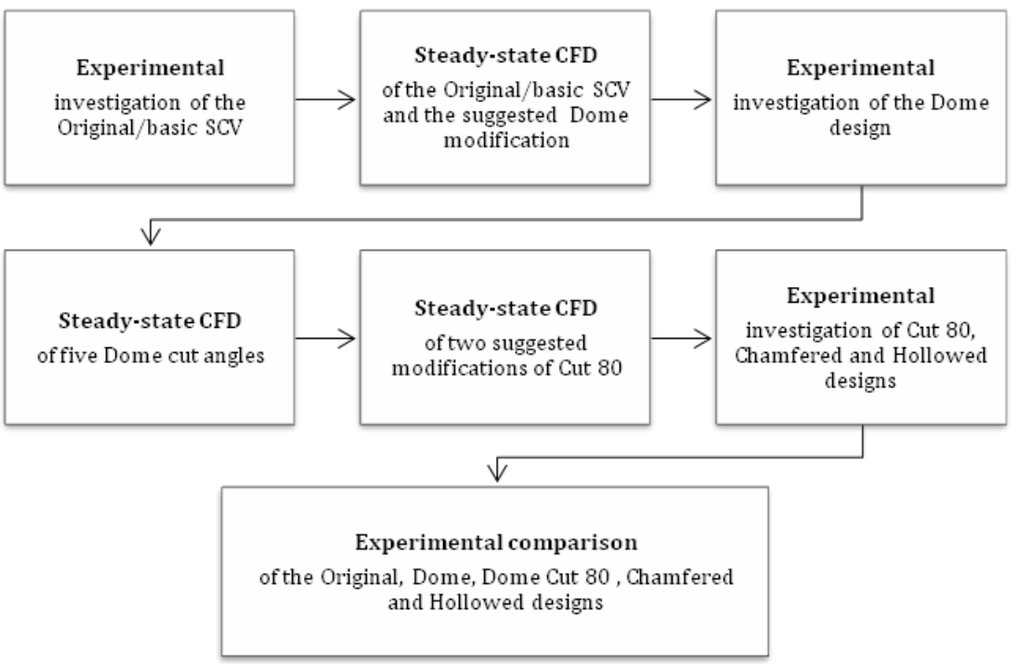

Fig. 2: Block diagram for the flow of results acquisition.

2. CASE STUDY

Two inches PVC wafer swing check valve is used in the present experimental work as the reference design. The reference/original SCV is shown in Figure 3.

3. NUMERICAL SIMULATIONS

The initial and boundary conditions of the steady-state simulations are obtained from the experimental data. Ansys Fluent v19.5 is used to perform a steady-state simulation at the fully open position of the SCV under the backward flow. The fully open position is chosen since it is the position where the closure starts. The steady-state simulations are used as a quick tool to decide which proposed design experiences larger hydraulic force, thus tends to close faster.

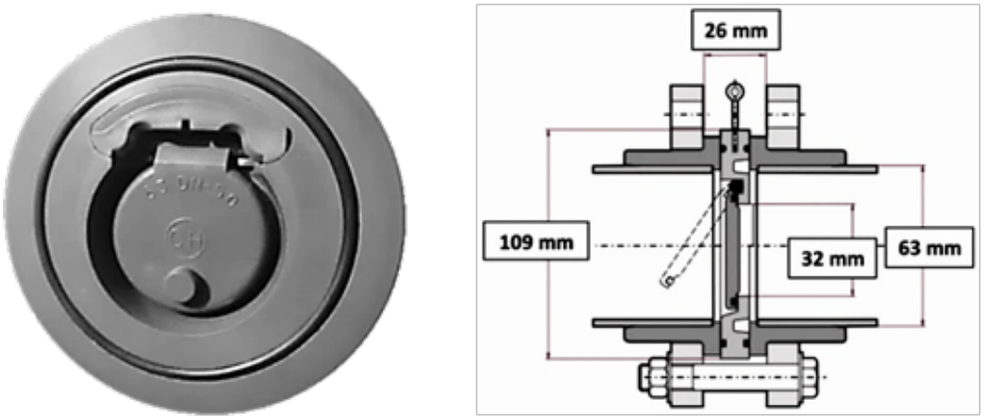

Fig. 3: The two inches wafer SCV.

According to the initial steady-state simulations, the most promising designs are selected for 3D printing and experimental investigation.

Boundary conditions were taken from experimental data of the original design as shown in Figure 4 where the inlet flow velocity is 0.17 [m/s] and the outlet is static pressure of 12.5 [kPa] gauge reading. No heat transfer is involved in the simulation, so the energy equation is ignored and the flow over walls is no-slip flow.The viscous model that is used is the k-ω SST turbulent model, since the Reynold's number of the flow is above the 4000:

d=0.05 m,
v=0.17 m/s,
ρ=998 kg/m^3,
Dynamic viscosity: $\mu = 8.9\times10^{-4}$ $Pa.s$

$$Re = \frac{\rho v d}{\mu} = 9531.46 \gg 4000$$

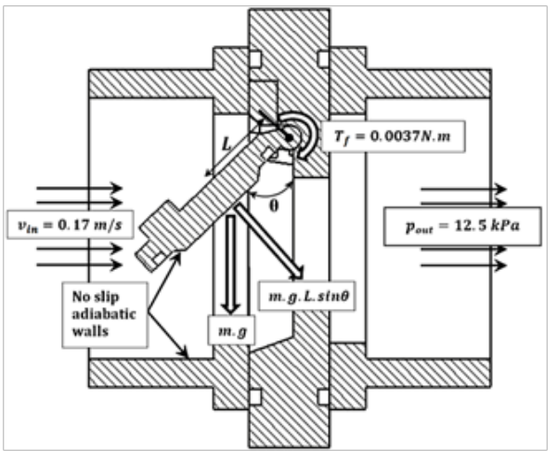

Fig. 4: Boundary conditions of the closing steady-state numerical simulation.

Before the simulation results are approved, mesh independent test was carried out for each design as shown in Table 1and Figure 5. The fifth level of refinement in Table 1and Figure 5was chosen so simulate with.

The mesh is divided into three volumes; the inlet and outlet pipes are sweepable and structured quadric mesh, while the valve volume is unstructured tetrahedron mesh with finer volume size of 1 [mm^3]. Five inflation layers are added to each wall to accurately capture the hydraulic effect on walls and the volume of that contained the hinge is excluded to simplify the mesh, Figure 6.

Table 1: Mesh independent test for the original design.

No. of cells	267492	325699	354001	360337	401664	500803
F_{hyd} [N]	-0.0051	-0.005742	-0.0071	-0.00698	-0.0071	-0.0071
Error %	---	10.98	18.61	1.03	1.15	0.21

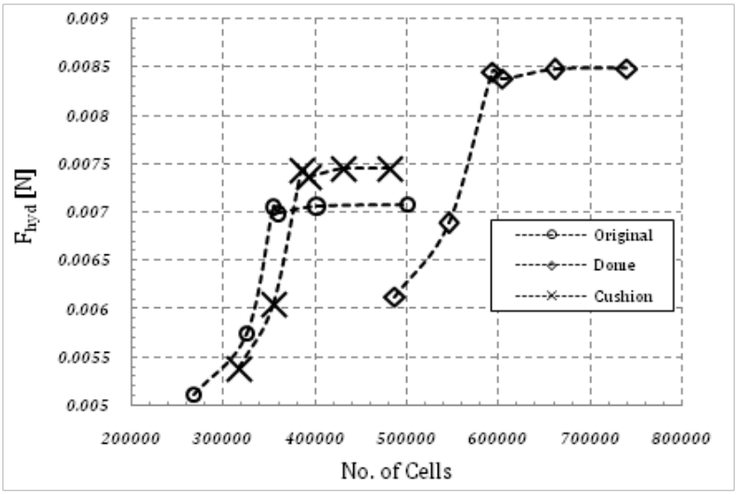

Fig. 5: Mesh independent test for the original, dome and cushion designs.

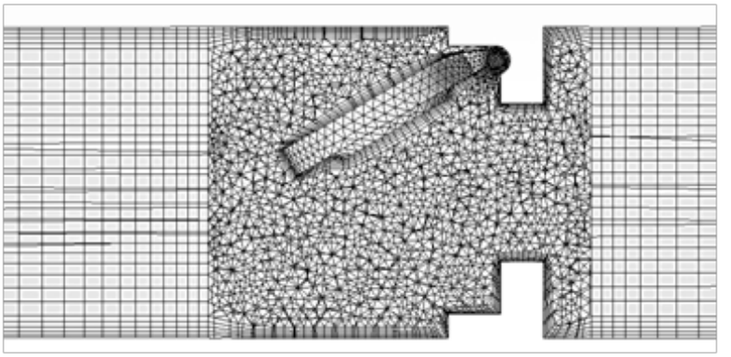

Fig. 6: The steady-state simulation mesh.

4. EXPERIMENTAL TESTING

A full experimental set-up is designed and developed to fulfil the requirements of several SCVs. The experiment is utilized to validate the mathematical model developed earlier by the authors[11].

4.1. Construction of the test rig

For any critical hydraulic system or/and any twenty four hours working system, two pumps are always connected in parallel and work alternatively. Inspired by Meng *et al.*[12] test rig design, the present test rig is constructed using two pumps configuration as shown in Figure 7.

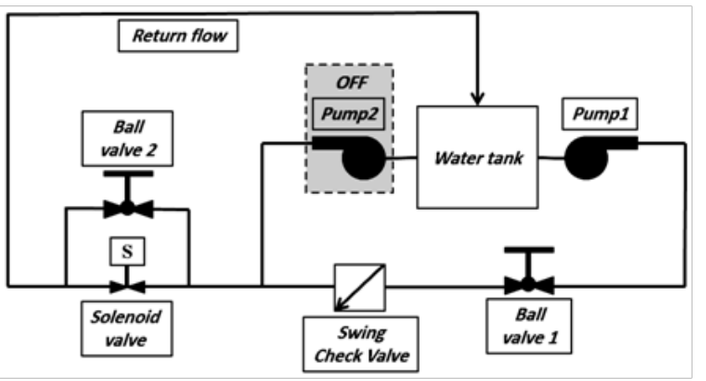

a) Opening the SCV.

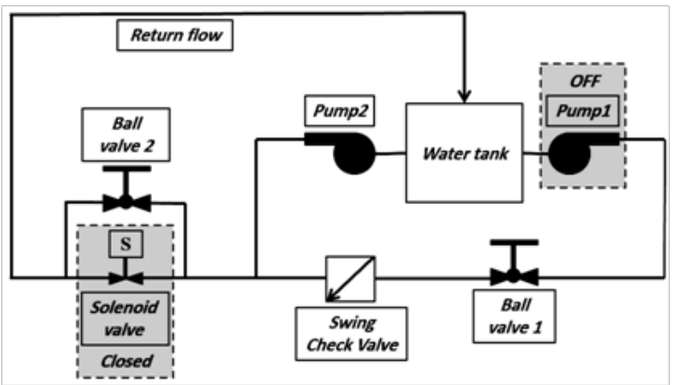

b) Closing the SCV.

Fig. 7: The proposed schematic of the SCV test rig.

Figure 7 shows that the SCV opens under the forward flow from "pump1", while "pump2"is switched off and the solenoid valve is not powered and normally opened. To close the SCV; "pump1" is switched off and both "pump2" and the solenoid valve are switched on instantaneously, consequently, water is forced to flow from "pump2" through the SCV. Figure 8 shows the 3D view with the dimensions in [cm] of the test rig. The description and quantity of each numbered component in Figure 8 are listed in Table 2. The final constructed test rig is shown in Figure 9.Both pumps are single phase, 220 [V] and 1 [hp]. While the solenoid valve that triggers the back flow is two inches size and closes in 0.1 [s], its operating pressure range is from 0.5 to 16 [bar].

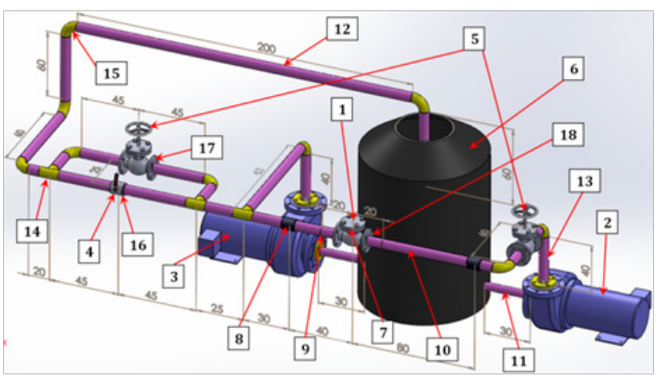

Fig. 8: Dimensions in [cm] and 3D view of test rig.

Table 2: Test rig components

Item	Swing check valve, 2"	Qty.
1	Swing check valve, 2"	1
2	Centrifugal pump "pump1", 1hp	1
3	Centrifugal pump "pump2", 1hp	1
4	Solenoid valve, 2", threaded ends, N.O.	1
5	Ball valve, 200-NPS2	2
6	Tank, 1 m3	1
7	Potentiometer	1
8	Flow meter, 2 in, threaded	1
9	Pressure transducer, 1/4 in, threaded	1
10	Acrylic Pipe, 2 in	2 m
11	PVC Pipe, 1 in	2 m
12	PVC Pipe, 2 in	9 m

13	Reducer, 1 to 2 in	4
14	Tee, 2 in	3
15	Elbow 90, 2 in,	9
16	Sleeve, 2 in	6
17	Union, 2 in	2
18	Acrylic Flange, 2 in	2
	Arduino Mega 2560	1

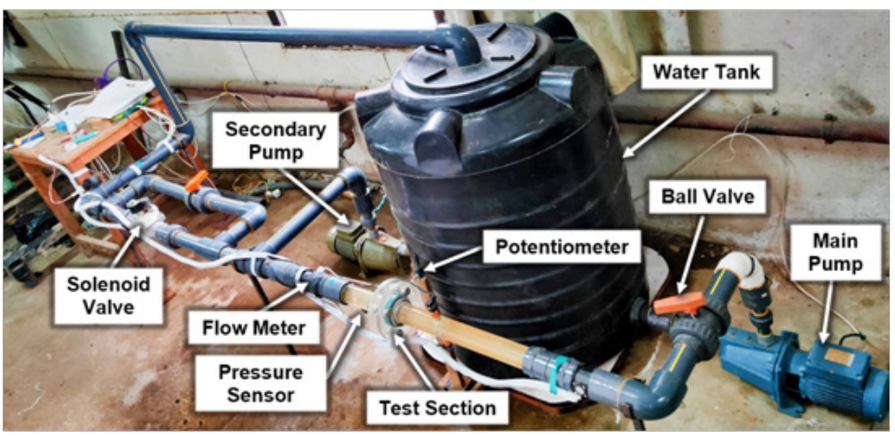

Fig. 9: The SCV physical test rig.

4.2. Test section design

The test section where the SCV is installed is made of transparent acrylic, so that the SCV can always be monitored as shown in Figure 10. The two acrylic pipes upstream and downstream of the SCV have lengths of 80 and 40 [cm] respectively, to maintain the installation constraints of 5D (five times the pipe diameter) and 2D free of obstacles distance upstream and downstream of the SCV. The flow meter is installed directly after the downstream acrylic pipe, and the pressure transducer is installed downward in the downstream pipe at a distance of 20 [cm] from the SCV, while the potentiometer is installed between the flanges aligned with the flapper's hinge.

Fig. 10: The transparent test section.

4.3 Fabrication and testing of the SCV

In order to measure the flapper's opening angle, a potentiometer is attached to the flapper's hinge through a hole in the valve body. To do so, the SCV is precisely drawn with SolidWorks software, and then the required holes are added to the 3D drawings. By having the original 3D model of the SCV on SolidWorks, the valve is ready to be fabricated via 3Dprinting using PLA (Polylactic Acid) plastic material(density =1250 kg/m^3) as shown in Figure 11.a.

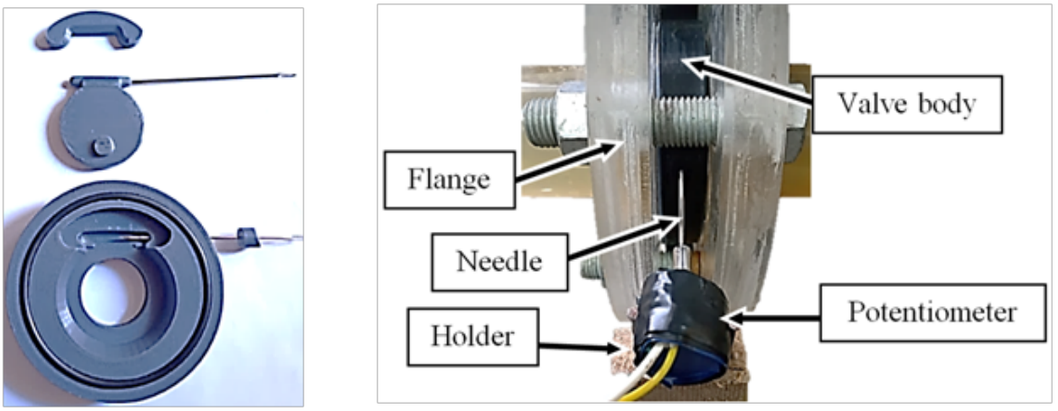

a) The 3D printed SCV. b) The potentiometer installed on the SCV.

Fig. 11: The final installation of the potentiometer.

Finally, the potentiometer is attached to the flapper's hinge via a long thin needle of radius of 2 [mm], as shown inFigure 11.b. The connecting hole in the valve body is filled by silicon material to prevent water leakage.

3D printing was selected as a manufacturing method over casting or machining for a number of reasons. Primarily, it is a rapid prototyping method that allows for the quick and easy creation of complex designs with intricate features. This was essential for the flapper design, which required a small hole to be created for the potentiometer needle. Additionally, 3D printing is a cost-effective manufacturing method, as it does not require the creation of expensive dies or tooling. This was also a major factor in the decision to use 3D printing, as the project involved testing a number of different flapper designs. Finally, 3D printing is a versatile manufacturing method that can be used to create a wide variety of objects, including prototypes, functional parts, and customized products. This made it the ideal manufacturing method for this project, as it allowed to create a variety of flapper designs and test them quickly and easily.

a) Pressure transducer b) Flow meter. c) Potentiometer

Fig. 12: Sensors that have been used in the experiment.

Sensors that are used to capture the performance of the SCV are: pressure transducer, flow meter and a potentiometer, Figure 12. An analogue pressure transducer is installed downstream the acrylic pipe at a distance of 20 [cm] from the SCV and on the down side of the pipe. The pressure transducer range is from 0 to 20 [bar] and its response time is 2 [ms].

The flow meter is an axial turbine type. The two inches flow meter is installed directly after the downstream acrylic pipe (40 [cm] from the SCV). It measures from 10 to 200 [L/min.] and withstands pressure up to 1.75 9 [Pa]. The potentiometer is used to measure the flapper's angle. It rotates up to 10 revolutions and the rotating torque is 0.0037 [N.m]. An Arduino Mega 2560 Rev3 microcontroller board is used as data acquisition hardware for measuring pressure, flow rate and angle.

5. RESULTS

As previously mentioned, the scope of the present work is to modify the traditional design of the SCV to close faster. So, the original design of the traditional SCV is experimentally tested first. Then, with the guidance of the steady-state numerical simulation, ten proposed designs will be investigated to decide which is more promising to be considered for 3D printing and experimental testing.

5.1. Experimental results of the Original SCV

The closing behaviour of the Original design is experimentally tested with more than 10 runs. The average values of these runs are shown in Figure 13.

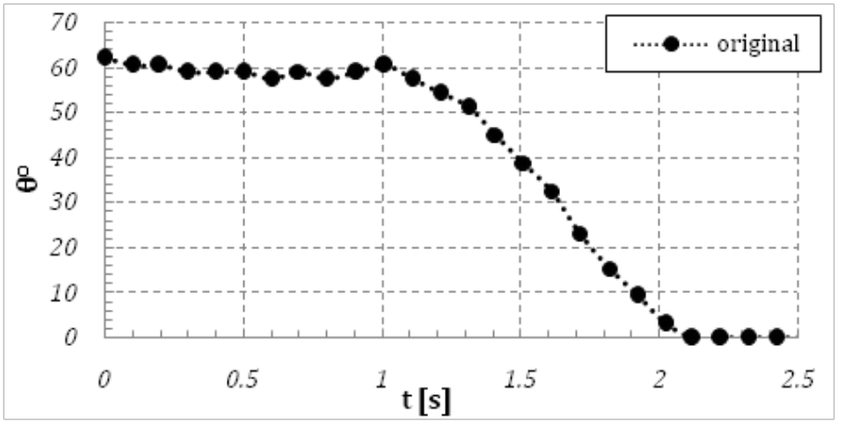

a) Angle versus time.

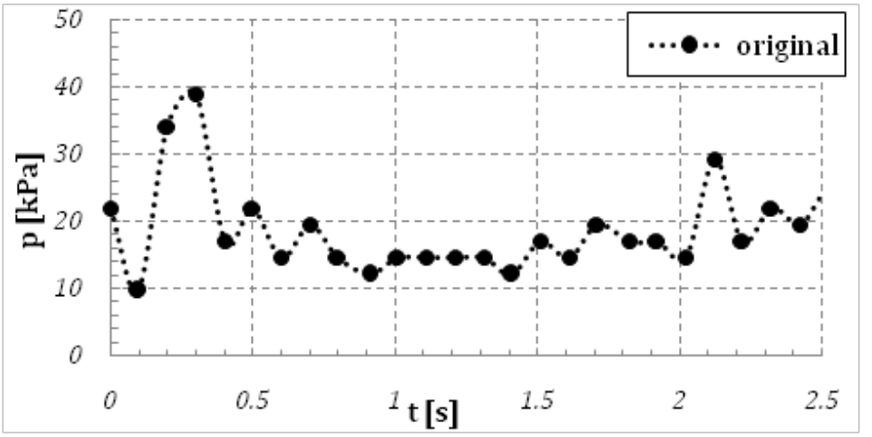

b) Pressure versus time.

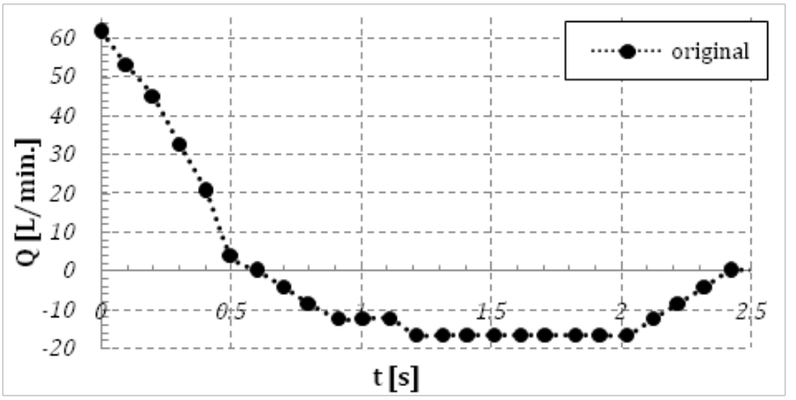

c) Flow rate versus time.

Fig. 13: Average values of the Original design closing parameters.

The mean value of the closing time "$\overline{t_c}$" and the standard deviation "σ_{tc}" are calculated as follows:

$$\overline{t_c} = \frac{\Sigma t_{c_i}}{n} = \frac{27.92}{13} = 2.147 \text{ [s]} \quad (1)$$

$$\sigma_{t_c} = \sqrt{\frac{\Sigma\left(t_{c_i} - \overline{t_c}\right)^2}{n-1}} = \sqrt{\frac{\Sigma\left(t_{c_i} - 2.147\right)^2}{13-1}} = 0.341 \text{ [s]} \quad (2)$$

$$t_c = 2.147 \pm 0.341 \text{ [s]} \quad (3)$$

Figure 13.a shows that the flapper does not instantaneously move after the solenoid closes, but it takes some time (1.1 [s]) before the flow is reversed and the flapper goes down when the hydraulic force changes its value and direction to overcome the inertia of the flapper, its friction in the hinge and with the fluid. Figure 13.b shows the first 39.5 [kPa] peak at t=0.3 [s], which is not due to valve closure, but due to the start of "pump2". The pressure peak due to the SCV closure occurs just when the flapper is fully closed (t=2.14 [s]), and its value is 29 [kPa]. Figure 13.c shows the flow rate (16.4 [L/min.]) and duration (1.6 [s]) of the reversed flow that occurs before the flapper is fully closed. The amount of flow rate recorded after the valve full closure can be attributed to the inertia of the turbine flow meter. Physical and geometrical properties of each design are listed in Table 3.

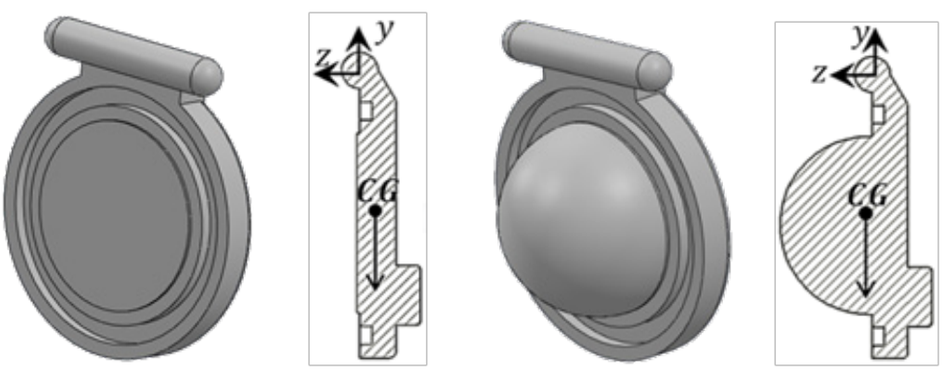

a) Original. b) Dome.

Fig. 14: The Original and Dome and designs of the flapper.

Table 3: Physical and geometric properties of Original and Dome designs.

	Original	Dome
Mass [g]	14.18	21.59
CG from hinge [mm]	y = -23.48, z = -2.6	y = -24.17, z = 0.53
Torque arm [mm]	23.62	24.18

Numerical simulations for Original and Dome designs

The steady-state CFD is used to investigate the suggested modifications of the SCV flapper before being manufactured and experimentally measured. The steady-state numerical simulation results of the closing hydraulic forces "F_{hyd}" on each flapper are shown in Figure 15.

The assisting closing hydraulic force on the Dome design is higher than Original design by 20% at the beginning of the closure.

The steady-state CFD results of the total pressure contours during the start of the closure for each design are shown in Figure 16.

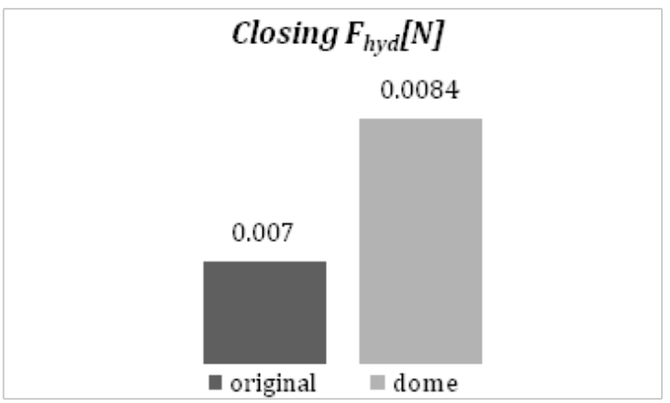

Fig 15: Closing hydraulic forces on Original and Dome designs.

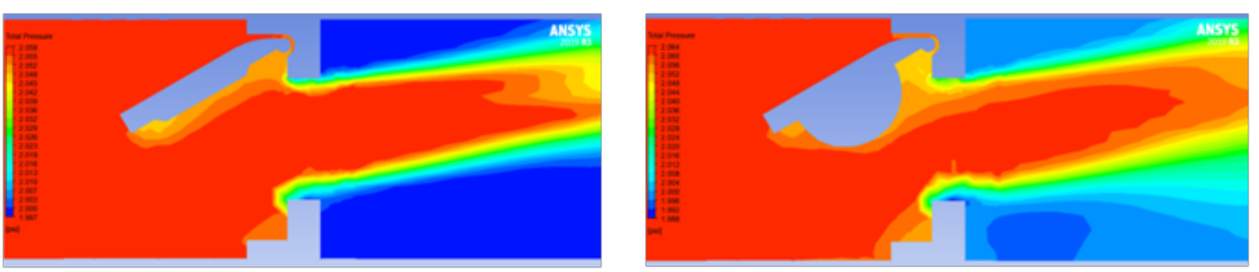

a) Original. b) Dome.

Fig. 16: CFD total pressure contours of the original, dome and cushion designs.

5.4. Experimental results of both Dome design

Dome design is also experimentally tested with more than 10 runs. The closing time for the Dome design is 1.51±0.13[s]. The average values of these runs are shown in Figure 17.

As expected, Figure 17.a shows that the Dome design closes faster (at 1.5 [s]) since it has the largest mass and the highest hydraulic force at the closure start position. Figure 17.b shows that the first pressure peak due to the start of "pump2" is almost identical in all designs, and the second pressure peak of each design occurs at the time at which the flapper is fully closed. The closing pressure of Dome design is only 8% smaller than the Original design, but the whole pressure range is very small and cannot be used as a judging parameter. The amounts of the reversed flow through each design are shown in Figure 17.c. The reversed flow seems to have no relation with the amount of the pressure rise, which is inconsistent with the popular

relation between the reversed flow and the pressure rise[13]. This can be attributed to the small operating pressure range of the whole experiment.

5.5. Numerical simulation for Dome sub designs

Since the Dome design shows the best closing performance, further investigation of the dome shape shall be more beneficial. A parametric steady-state CFD study is implemented on the dome design by making a chamfered cut opposing the backward flow during closure in order to enclose more fluid, subsequently increase the closing hydraulic force on the flapper.

Figure 18 shows the five cut modifications to the Dome design, where the chamfer cut angle ranges from 0 to 100 degrees with a step of 20 degrees.

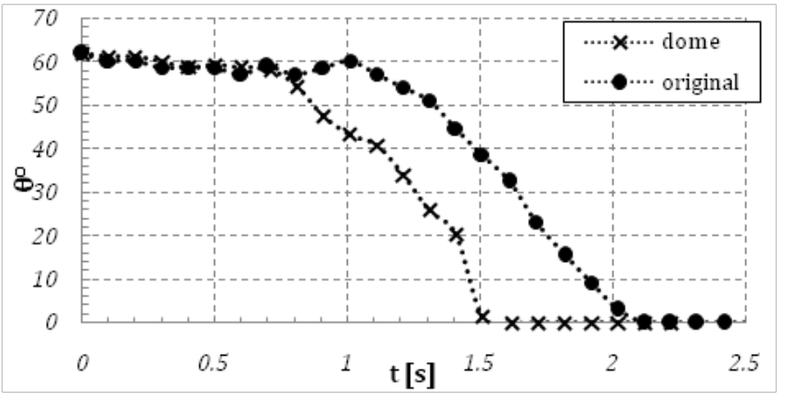

a) Angle versus time.

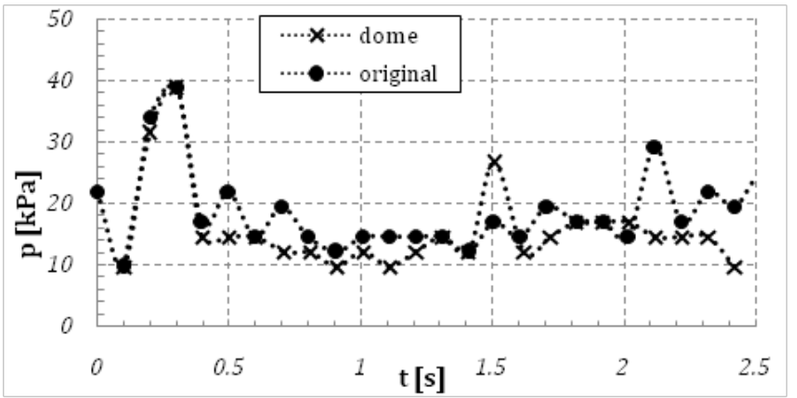

b) Pressure versus time.

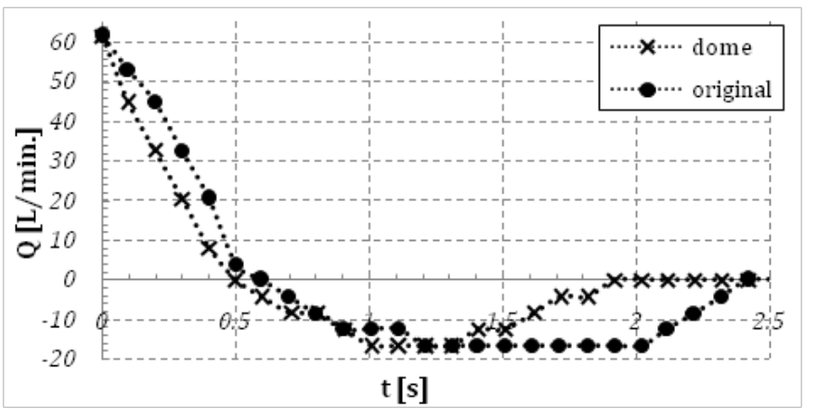

c) Flow rate versus time.

Fig. 17: Average values of the Original versus Dome designs closing parameters.

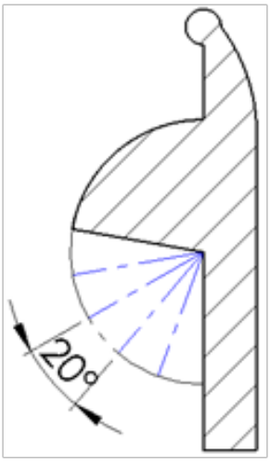

Fig. 18: Different cut angles to the Dome design.

Results of hydraulic force value on each modification at the fully opening position are shown in Figure 19.

The Dome cut 80 modification experiences the largest increase in hydraulic force, with a percentage increase of 3.34% than the full Dome design. The percentage increase in its hydraulic force with respect to the Original flapper design is 23.76%, which makes this design worth to be experimentally investigated. Two other suggested modifications to the SCV flapper are emerged from Dome cut 80 design and shown in Figure 20. The first modification is to hollow the remaining dome volume so that it can collect much more back flow aiming to increase the closing hydraulic force. The another modification is chamfering the back spherical shape of the Dome cut 80 design aiming to increase the pressure drop behind, consequently increase the pressure different across the flapper and the closing hydraulic torque. Contours of total pressure of the three newly suggested designs are shown in Figure 21.

The closing hydraulic force of the Dome cut 80 modifications as well as theDome and Original designs are shown in Figure 22.

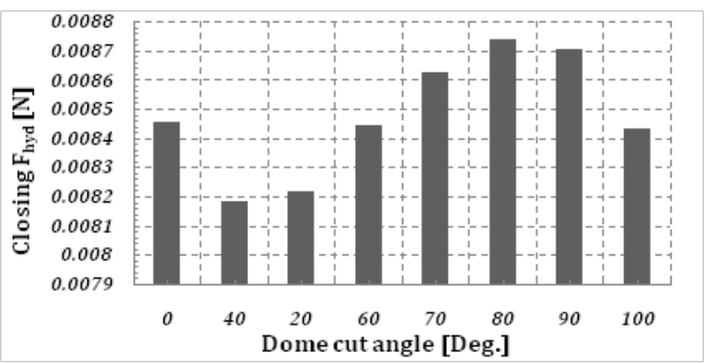

Fig. 19: Closing Hydraulic force on different Dome cut angle.

a) Cut 80. b) Hollow 80. c) Chamfer 80.

Fig. 20: The Dome cut 80 modifications.

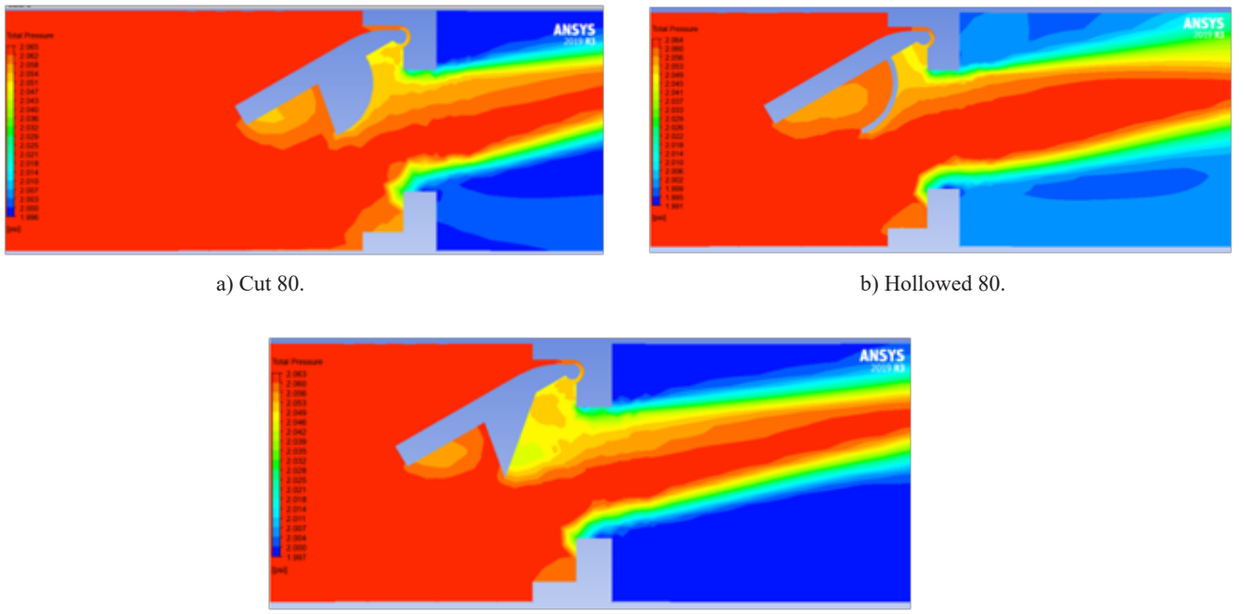

a) Cut 80.

b) Hollowed 80.

c) Chamfer 80.

Fig. 21: CFD total pressure contours of the three dome cut 80 modifications.

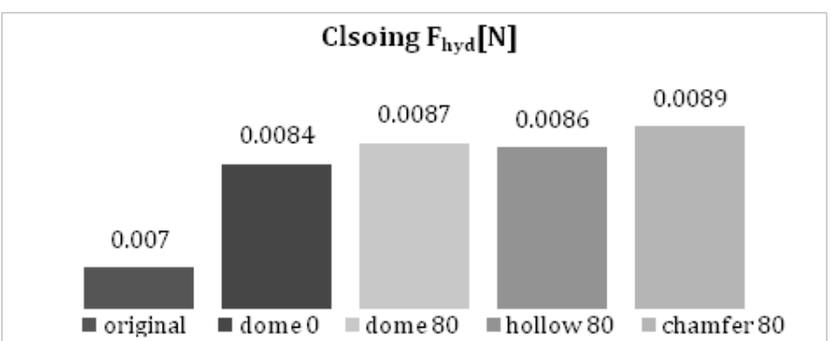

Fig. 22: Closing hydraulic force on Original and Dome sub designs.

Though the improvement in the hydraulic closing forces on the Dome cut 80 modifications ranges from 23.7% to 26.8% than the Original design, but the numerical simulation is only a steady-state one and the actual transient performance may vary. So, the three Cut 80 modifications are 3D printed to be experimentally investigated versus the Original design.

5.6. Experimental results of the selected Cut 80 modifications

As well as the other experimental results, the closing behaviours of the Cut 80 modifications are experimentally tested with more than 10 runs. The closing times for the Cut 80, Hollow 80 and Chamfer 80 designs are 2.96 ± 0.71[s], 1.86±0.13[s] and 2.26±0.26[s] respectively. The average values of these runs are shown in Figure 23.

Figure 23.a shows that the Hollow 80 design closes the fastest (at 1.85 [s]), which is due to its hollowed design that collects the back flow and increases the closing hydraulic force on it. The Chamfer 80 closes slower than the Hollow 80 design (2.26 [s]), but faster than the normal Cut 80 design (2.95 [s]) because of the pressure drop behind the cut that causes higher pressure drop and larger hydraulic force than the normal Cut 80 design. Figure 23.b shows that the SCV closure pressure peaks of the Hollow, Chamfer 80 and Cut 80 modifications are 27, 24 and 29 [kPa] respectively. Figure 23.c also shows that the faster the valve closure, the less reversed flow passes through the valve.

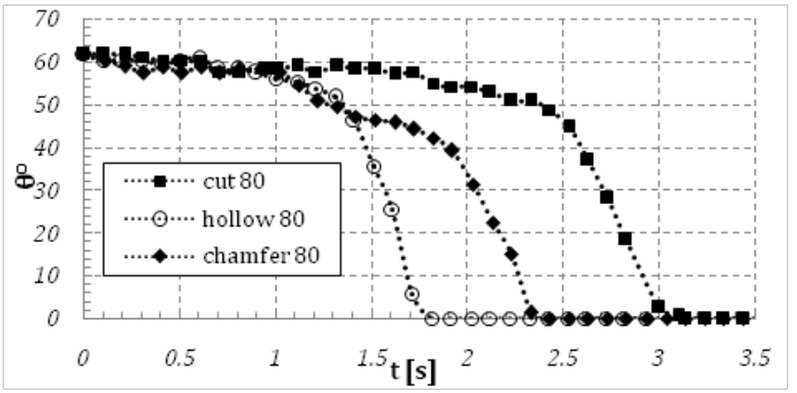

a) Angle versus time.

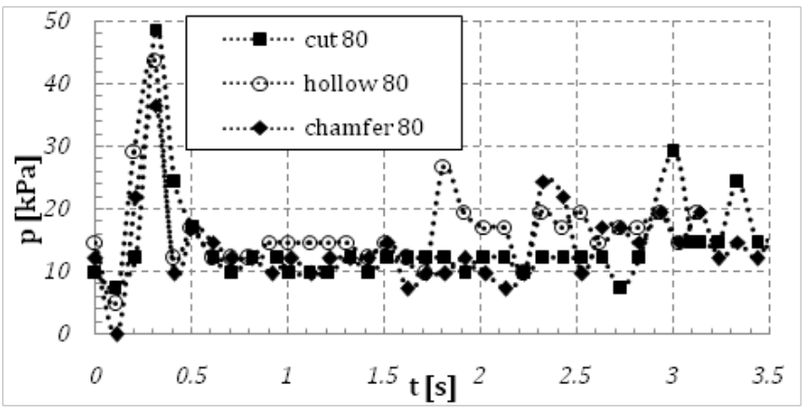

b) Pressure versus time.

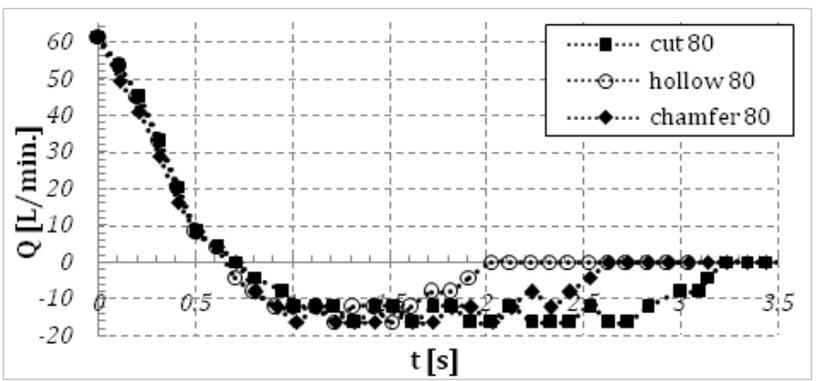

c) Flow rate versus time.

Fig. 23: Average values of Dome cut 80 designs closing parameters.

5.7. Summary

The five flapper designs (the Original design and the five modified designs) that are 3D printed and experimentally investigated are shown in Figure 24.

Figure 25 summarizes the angle-time performance of the five designs that are experimentally investigated, where the Dome design closes the fastest followed by the Hollow 80 before the Original design.

closing time of each design can be also presented in bar chart as shown inFigure 26

Figures 25 and 26 show that the Dome design closes first at t=1.51 [s] (29.7% faster than the Original design), then the Hollow 80 design at t= 1.86 [s] (13.4% faster than

the Original design). Here is an important notice that the Hollow 80 design closes faster because of its shape and not because of its weight like the Dome design, since the Hollow 80 design is 1.12% lighter than the Original design, and it has the least mass among the modified designs. Figure 27 shows the mass of each design.

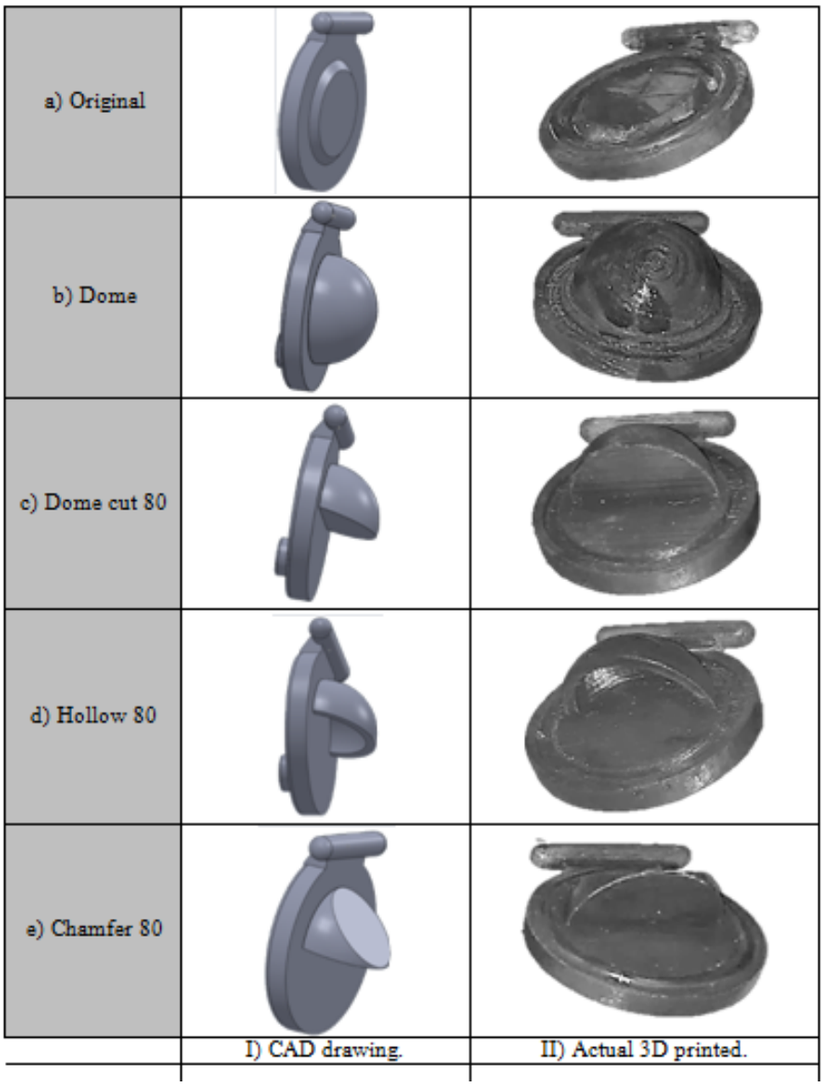

Fig. 24: The five flapper designs that were experimentally tested.

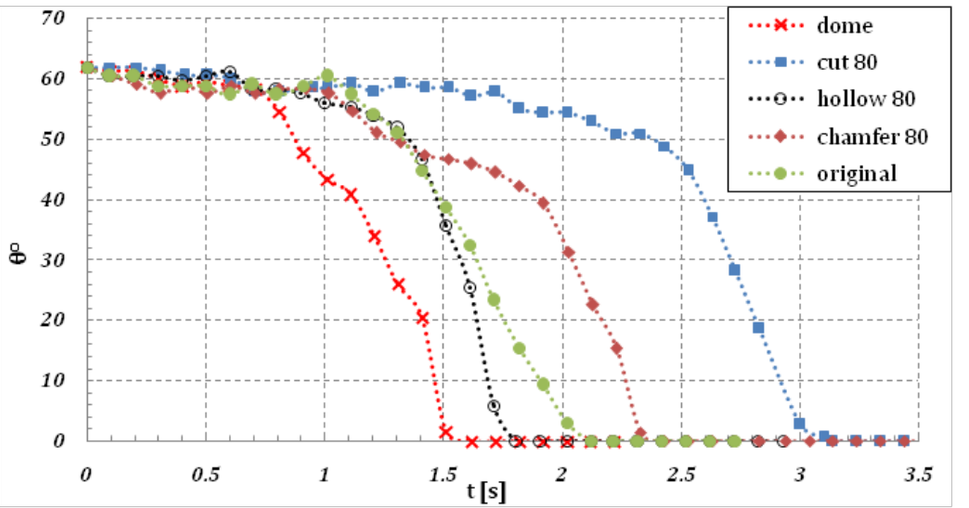

Fig. 25: Angle versus time of all models.

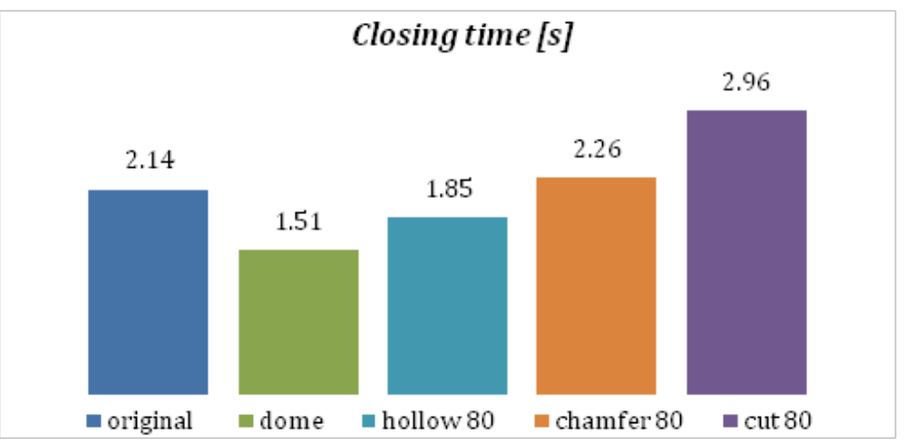

Fig. 26: Closing time for each design

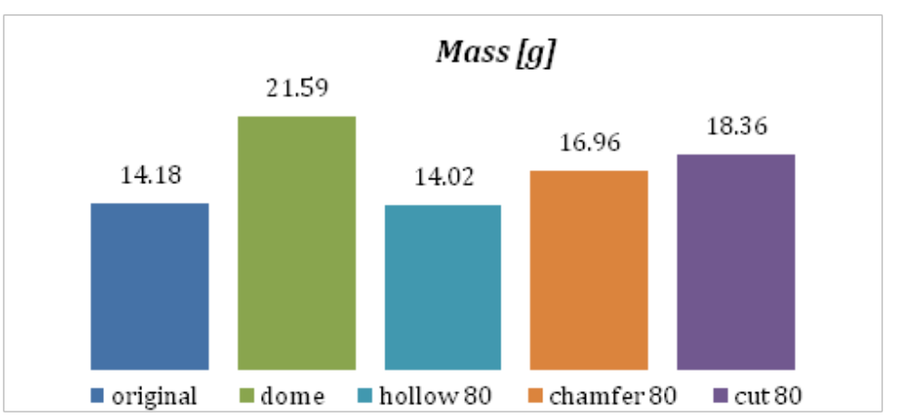

Fig. 27: Mass of each design.

Figure 28 shows the static pressure in the system versus time.

The first pressure peaks are due to "pump2" sudden start, and the latter pressure peaks are due to the SCV closure. Pressure peaks due to the closure of the SCV for each design, are comparably small as shown in Figure 29, and the differences among them are also very small. That is why pressure rise in the current experiment cannot be used as judgmental parameter.

The amount of reversed flow through each model before it is fully closed is inversely proportioned to its closing time as shown in Figure 30.

Finally, the amounts of the reversed flow Q r pass through each design before it is fully closed are shown in Figure 31.

The amount of the reversed flow is reduced by 29.3% and 15.5% for both Dome and Hollow 80 designs respectively compared to the Original design.

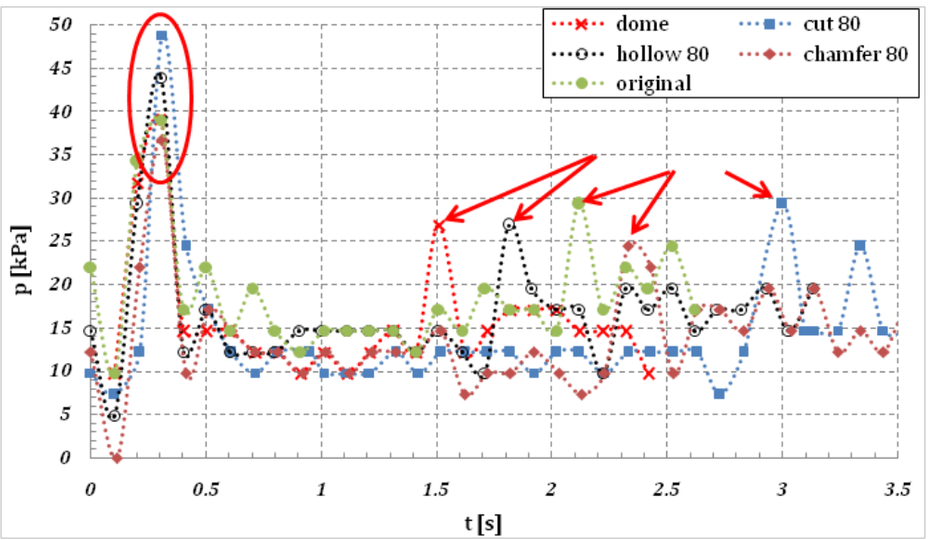

Fig. 28: Pressure versus time for all models.

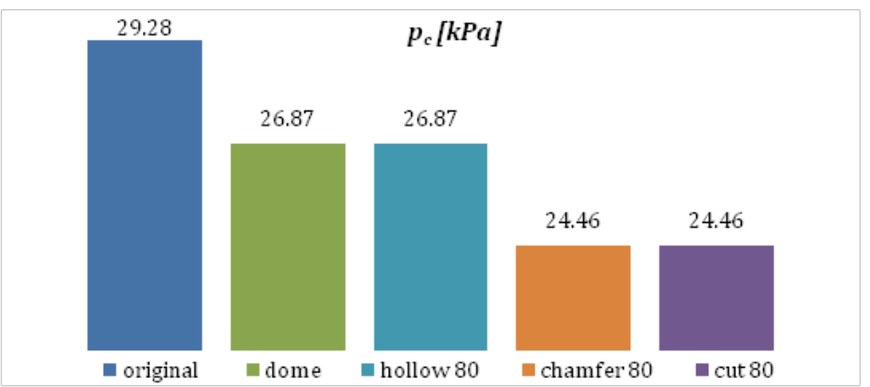

Fig. 29: Pressure peaks due to SCV closure of all designs.

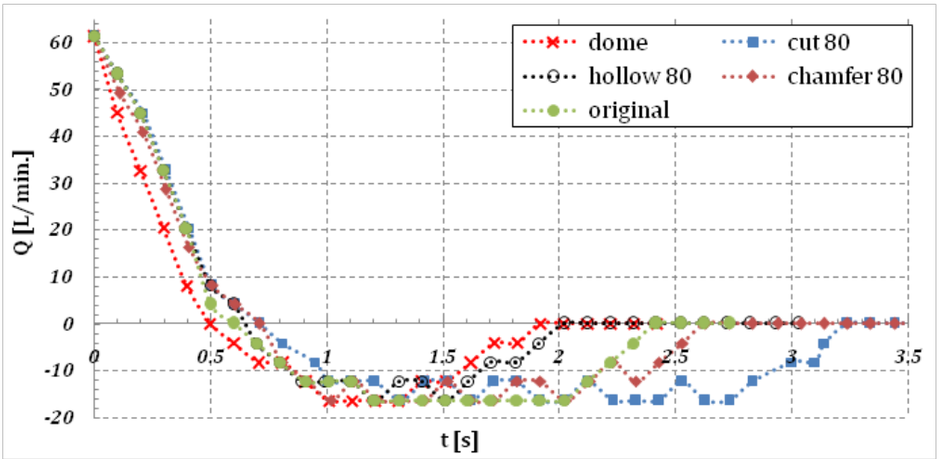

Fig. 30: Flow rate versus time for all models.

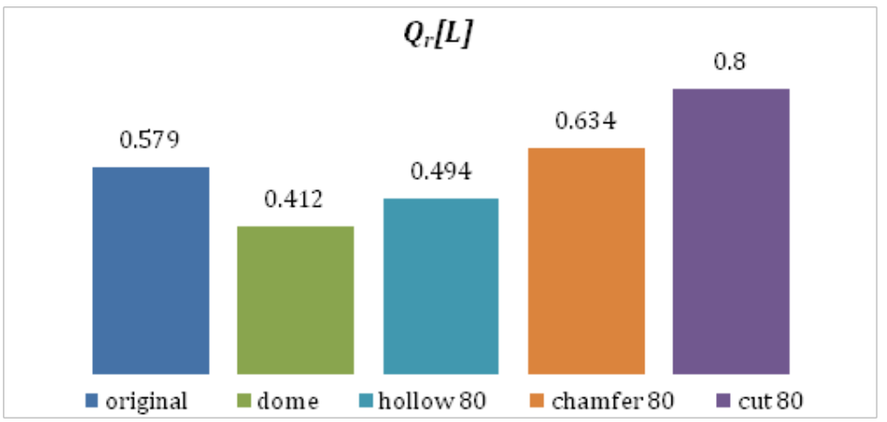

Fig. 31: Maximum reversed flow through each design.

6. CONCLUSION

The Original/basic design of the SCV closes in 2.14±0.34 [s], while the Dome design closes the fastest in 1.51±0.13 [s] (29.7% faster than the Original basic design). The closure time of the Dome is the shortest because it has the largest mass among the others (52.25% heavier than the Original design). The Hollow 80 design closes the second in 1.86±0.13 [s] (13.4% faster than the Original basic design) not because of its mass (its mass is 1.12% lighter than the Original design) but since it has a unique shape that collects the reversed flow and enlarge the value of the closing hydraulic force on it. Therefore, in plastic and light materials as well as small SCV sizes, the Dome design may be an optimum choice. While in metallic heavy materials and large SCV sizes, the Hollow 80 design may be better since the percentage increase of the mass is very small.

Flow rate curves show that the amount of the reversed flow that passes through the valve before it goes fully closed increases with the increase of the closing time of the valve. Both Dome and Hollow 80 designs reduce the amount of reversed flow by 29.3 and 15.5% respectively.The two designs of the Dome and Hollow 80 reinforce the idea that the traditional plain design of the SCV shall be modified to give better operating performance.

7. Nomenclatures

AFWS	Auxiliary feed water system
CFD	Computational fluid dynamics
CG	Centre of gravity
D	Diameter of the flapper's disc, m
F_	Force, N
g	Gravitational acceleration, m/s^2
hp	Horse power
m	Mass, kg
min.	Minute
N.O.	Normally opened

n	Number of times
OPR	Optimized power reactor
p	Pressure, Pa
Q	Flow rate, m^3/s
rps	Revolution per second
SCV	Swing check valve
t	Time, s
V	Voltage, V
v	Flow velocity, m/s
θ	Flapper's opening angle, degree
σ	Standard deviation
c	Closing
hyd	Hydraulic
r	Reversed

7. REFERENCES

[1] H. D. Haynes, "Evaluation of Check Valve Monitoring Methods," Nucl. Eng. Des., vol. 134, pp. 283–294, 1992.
[2] K. L. Mcelhaney, "An Analysis of Check Valve Performance Characteristics Based on Valve Design," Nucl. Eng. Des., vol. 197, pp. 169–182, 2000.
[3] P. Griffith and J. C. Sununu, "Wear in Check Valves Due to Flow Induced Motion," Nucl. Eng. Des., vol. 115, pp. 323–330, 1989.
[4] J. Lee, M. Lee, J. Kim, V. Luk, and Y. Jung, "A Study of the Characteristics of the Acoustic Emission Signals for Condition Monitoring of Check Valves in Nuclear Power Plants," Nucl. Eng. Des., vol. 236, pp. 1411–1421, 2006, doi: 10.1016/j.nucengdes.2006.01.007.
[5] B. Ziegler, P. Coppolani, and J. L. Garcia, "Dynamic Behavior of Check Valves and Safety Valves with Fluid Interaction," Nucl. Eng. Des., vol. 124, pp. 391–401, 1990.
[6] H. Lim, J. Park, and S. Jang, "Development of a Swing Check Valve Model for a Low Velocity Pipe Flow Prediction," Nucl. Eng. Des., vol. 236, pp. 1051–1060, 2006, doi: 10.1016/j.nucengdes.2005.12.004.
[7] S. Li, Y. Hou, and L. Li, "Dynamic Characteristics of Swing Check Valve Based on Dynamic Mesh and UDF," Appl. Mech. Mater., vol. 324, 2013, doi: 10.4028/www.scientific.net/AMM.321324.86-.
[8] H. G. Knoedler, "A Systems Engineered Approach Towards Improved Safety and Performance of Valves," Nucl. Eng. Des., vol. 134, pp. 277–282, 1992.
[9] H. Mochizuki, "Evaluation Method of Check-Valve Integrity during Sudden Closure Using Thermal-Hydraulic and Structural Analyses," Nucl. Eng. Des., vol. 200, pp. 273–284, 2000.
[10] S. M. Shin, D. S. Kim, and H. G. Kang, "Power-Operated Check Valve in Abnormal Situations," Nucl. Eng. Des., vol. 330, no. December 2017, pp. 28–35, 2018, doi: 10.1016/j.nucengdes.2018.01.017.
[11] A. M. El-zahaby, M. Y. Zakaria, Y. A. F. El-samadony, and A. Ibrahim, "Vibration caused by swing check valve closure," 2019, doi: 10.1088899-1757/X/610012050/1/.
[12] H. Meng, Y. Liu, and Y. Li, "Experiment on Water Hammer Protection Performances of the Shuttle Check Valve in Multi-pump Parallel Connection System," Appl. Mech. Mater., vol. 192, pp. 37–41, 2012, doi: 10.4028/www.scientific.net/AMM.192.37.
[13] W. Rahmeyer, "Dynamic Flow Testing of Check Valves," the Nuclear Industry Check Valve Group. St. Petersburg, Florida, pp. 1–9, 1996.